Author Manuscript

Author Manuscript

Author Manuscript

Author Manuscript

HHS Public Access

Author manuscript

Chembiochem. Author manuscript; available in PMC 2016 August 17.

Published in final edited form as:

Chembiochem. 2015 August 17; 16(12): 1725–1729. doi:10.1002/cbic.201500278.

Super-Resolution Imaging and Quantitative Analysis of Membrane Protein/Lipid Raft Clustering Mediated by Cell Surface Self-Assembly of Hybrid Nanoconjugates

Jonathan M. Hartley[a],**, **Te-Wei Chu**[b],**, **Eric M. Peterson**[c], **Rui Zhang**[b], **Jiyuan Yang**[b], **Joel Harris**[c], and **Jindřich Kopeček**[a],[b]

Jonathan M. Hartley: jindrich.kopecek@utah.edu

[a]Department of Bioengineering University of Utah 20 S. 2030 E., Rm. 108, Salt Lake City, UT 84112

[b]Department of Pharmaceutics and Pharmaceutical Chemistry University of Utah 30 S 2000 E Room 301, Salt Lake City, UT 84112

[c]Department of Chemistry University of Utah 315 S 1400 E, RM 2020, Salt Lake City, UT 84112

Abstract

Super-resolution imaging was used to quantify organizational changes in the plasma membrane after treatment with hybrid nanoconjugates. The nanoconjugates crosslinked CD20 on the surface of malignant B cells thereby inducing apoptosis. Super-resolution images were analyzed using pair-correlation analysis to determine cluster size and to count the average number of molecules in the clusters. The role of lipid rafts was investigated by pre-treating cells with a cholesterol chelator and actin destabilizer to prevent lipid raft formation. Lipid raft cluster size correlated with apoptosis induction after treatment with the nanoconjugates. Lipid raft clusters had radii ~200 nm in cells treated with the hybrid nanoconjugates. Super-resolution images provided precise molecule location coordinates that could be used to determine density of bound conjugates, cluster size, and number of molecules per cluster.

Keywords

nanomedicine; dSTORM; nanotechnology; Self-assembly

Synthetic polymers bound to drugs or proteins provide advantages over small molecule therapeutics such as: improved biodistribution and lower toxicity.[1] For example, polyethylene glycol has been attached to therapeutic proteins to increase blood circulation time and decrease immunogenicity. The monomer *N*-(2-hydroxypropyl)methacrylamide

Correspondence to: Jindřich Kopeček.

**J.M. Hartley and T.-W. Chu contributed equally to this work.

Competing Interests

J.K., J.Y. and T.-W.C. are inventors on a pending US patent application (PCT/US2014/023784; assigned to the University of Utah) related to this work. J.K. is Chief Scientific Advisor and J.Y. Scientific Advisor for Bastion Biologics. Otherwise, the authors declare no competing financial interests.

Supporting information for this article is given via a link at the end of the document.

Author Manuscript Author Manuscript Author Manuscript Author Manuscript

(HPMA) can be polymerized using reversible addition-fragmentation chain transfer (RAFT), atom transfer radical polymerization (ATRP), and conventional radical polymerization into a hydrophilic biocompatible polymer.[2] Polymeric nanomedicines have progressed from simply altering biodistribution to performing complex biological functions in vivo such as self-assembly to induce apoptosis in cancer cells.[3] Rational nanomedicine design can be facilitated by an improved characterization of the molecular-level interactions between cellular membranes and nanoconstructs.[4]

Traditional tools for studying molecular-level interactions between cell membrane components (proteins, lipids, cholesterol) and polymer therapeutics are limited. Confocal microscopy is limited by optical diffraction, which prevents characterization of structures below ~200 nm; however, new optical imaging techniques can reach resolutions of 10 nm [5] by controlling fluorophore activation and emission. These super resolution imaging techniques—photoactivatable localization microscopy (PALM), stochastic optical reconstruction microscopy (STORM), and direct STORM (dSTORM)—are broadly categorized as localization microscopy techniques.[6] These techniques control the activation and emission of fluorophores so that sparse subsets of molecules are activated and precisely localized in an individual frame. Localization microscopy provides the spatial coordinates for all localized molecules in the image, which can then be analyzed using biophysical analysis tools such as pair-correlation analysis to extract quantitative physical characteristics in the image, like size and cluster spacing.[7]

In 2012, Non-Hodgkin's lymphoma (NHL) resulted in ~400,000 new cases and ~200,000 deaths worldwide.[8] The majority (85%) of NHL cancers are of B cell origin. B cells express the non-shedding and non-internalizing membrane protein CD20—a 33 kDa protein that is associated with lipid rafts.[9] Crosslinking of CD20 results in activation of tyrosine kinases, release of intracellular stores of calcium ion, activation of caspase signaling, and initiation of apoptosis.[10] Monoclonal antibodies directed toward CD20 (e.g. Rituximab) have proven effective in treating NHL, but half of treated patients do not respond to treatment; therefore improved medicines are needed.

To address the limitations of current NHL treatments, we developed a new therapeutic paradigm utilizing hybrid nanomaterials. Our therapeutic employs two complementary hybrid nanoconjugates that bind to CD20 and self-assemble causing CD20 crosslinking (Figure 1).[3c] The two nanoconjugates are comprised of three main components: 1) The complementary morpholino oligonucleotide analogs MORF1 and MORF2, which hybridize with picomolar affinity; 2) An anti-CD20 Fab′ fragment from the mAb 1F5, which is bound to MORF1; and 3) A linear polyHPMA bearing multiple copies of MORF2 for hyper-crosslinking of the Fab′-MORF1 conjugates bound to CD20. In this study, we sought to clarify the effects of nanoconjugate self-assembly on protein distribution in the plasma membrane using super resolution microscopy and pair-correlation analysis. Our therapeutic system can be administered in two different ways: 1) Consecutive, where Fab′-MORF1 is added to the cells or injected into mice first then, an hour later (or other optimized time), the P-MORF2 is added; or 2) Pre-mixed, where the conjugates are mixed together prior to addition to cells or injection into mice.

Author Manuscript Author Manuscript Author Manuscript Author Manuscript

Bioconjugation of the Fab′ fragment to MORF1 was accomplished by first modifying the MORF1 oligo with the heterobifunctional linker SMCC (succinimidyl 4-(N-maleimidomethyl)cyclohexane-1-carboxylate) and then mixing Fab′-SH with the resulting MORF1-mal (Scheme 1A). The lysine residues on the Fab′-MORF1 conjugate were fluorescently labeled with NHS-functionalized Alexa Fluor 647.

The P-MORF2 conjugate was prepared using RAFT copolymerization of HPMA with an amine reactive comonomer (MA-GG-TT). The thiazolidine-2-thione (TT) groups were incorporated into the HPMA backbone to make P-TT with a Mw of 136 kDa and a PDI of 1.15. The P-TT polymer was then conjugated to MORF2-NH_2. The conjugates were characterized as described previously.[3c]

Rituximab is known to be dependent on lipid raft integrity to activate calcium entry into the cell and caspase activation.[11] Lipid rafts play a vital role in cell signaling, especially in apoptosis.[12] It is still unknown whether the nanoconjugates require lipid raft platforms to induce apoptosis and how the conjugates alter the lateral organizing of proteins in the membrane. We used methyl-β-cyclodextrin (MβCD) to extract cholesterol, a component of lipid rafts, from the cell membrane[13] and Latrunculin B (LatB) to disassemble cortical actin.[14]

The role of cholesterol and actin were investigated by pretreating the cells with MβCD and LatB respectively. As a positive control, the 1F5 mAb was used along with a secondary goat anti-mouse antibody to hypercrosslink the bound 1F5 (mAb +2°Ab). The mAb+2°Ab ($p = 0.01$), Rituximab ($p = 0.00007$) and consecutive ($p = 0.00002$) groups significantly induced apoptosis above the untreated control (Figure 2A). The nanoconjugates (consecutive group) induced significantly greater levels of apoptosis than the clinically used antibody Rituximab (Figure 2A). In all cases, with the exception of the mAb+2°Ab group pre-treated with MβCD, apoptosis was significantly inhibited (Figure 2A and 2B).

All treatments showed significant apoptosis inhibition when pretreated with LatB (Figure 2B). Therefore, cortical actin stability enhanced the efficacy of Rituximab and the hybrid nanoconjugates. The prominent role that lipid rafts play in the induction of apoptosis by the nanoconjugates supports the model proposed by Deans et al., where lipid raft clustering allows transactivation of src-family kinases.[9] Nanoconjugate self-assembly and hypercrosslinking of CD20 appears to indirectly induce apoptosis through a similar lipid raft clustering mechanism. The cytoskeleton plays a critical role in plasma membrane organization through interactions with transmembrane proteins,[15] so destabilization of cortical actin by LatB results in randomization of lipid raft components in the plasma membrane. The nanoconjugates showed similar decreases in apoptosis to Rituximab after actin destabilization and cholesterol depletion indicating that the conjugates exhibit mechanistic behavior similar to Rituximab in vitro.

In order to validate the lipid raft-clustering hypothesis, we imaged CD20 and lipid raft clusters after nanoconjugate treatment. We used dSTORM to provide super resolution images of Raji cellular membranes subjected to various treatments. Lipid rafts were tracked using Alexa Fluor 555 conjugated to cholera toxin B. CD20 distribution was tracked using

Author Manuscript Author Manuscript Author Manuscript Author Manuscript

fluorescently labeled Fab′-MORF1-AF647. Pre-treatments with MβCD and LatB were performed to determine if there were structural changes in the membrane organization and if they correlated with apoptosis induction.

Cell membranes treated with the nanoconjugates (Figure 3A) showed increased clustering of CD20 over cells treated with Fab′-MORF1 only (Figure 3C). Cells pretreated with LatB (Figure 3e) and MβCD (Figure 3G) and then with the Fab′-MORF1-AF647 (1 h) followed by P-MORF2 (1 h) showed similar clustering as cells treated with Fab′-MORF1 only.

To determine the average cluster size and number of localizations per cluster we used pair-correlation analysis. Sections of the 2D images were selected for pair-correlation analysis in Matlab (Figure 3). Measured pair-correlation functions ($g(r)^{peaks}$) were fit to the theoretical function

$$g(r)=\frac{\exp(\frac{-r^2}{4\sigma^2})}{4\pi\sigma^2\rho}+A\exp\left(\frac{-r}{\xi}\right)+1 \quad \text{Equation (1)}$$

where r is the radial offset in nm, σ is the standard deviation of the localization precision (Figure S3), ρ is the average density of localizations in the image, and ξ is the characteristic decay, which is approximately the average cluster radius. Values of ξ were determined for images of the lipid rafts and CD20 by fitting the pair-correlation function to Equation 1 (Figure 3). Lipid raft cluster size was significantly larger than nontreated ($p = 0.02$), Fab′-MORF1 ($p = 0.01$), and MβCD ($p = 0.01$) and LatB ($p = 0.03$) pretreated cells (Figure 4C). The average density of Fab′-MORF1 bound to the surface in all the various treatments was $\rho = 170$ molecules/μm^2, assuming a cell diameter of 10 μm that gives approximately 50,000 molecules of Fab′-MORF1 bound to the surface of each B cell. This number is a lower estimate as it is possible that only a fraction of the bound dye was imaged. However, the calculated number of bound Fab′-MORF1 is reasonable given that CD20 resides as dimers and tetramers in the plasma membrane so due to steric hindrance not all CD20 will bind to Fab′-MORF1. The average number of CD20 on a B cell is 250,000 per cell.[16]

The CD20 cluster sizes were not significantly different (Figure 4C). The number of localizations per cluster can be approximated using the equation $N^{cluster} = 2A\pi\xi 2\rho$. The mean number of molecules in the lipid raft clusters of nanoconjugate-treated cells was approximately 5 times greater than the controls, but due to high variability and small sample size the difference cannot be confirmed as significant. The shape of the pair-correlation curves of the lipid rafts revealed differences in cluster size. Figures 4A and 4B contain pair-correlation functions that were normalized in order to compare the shape of the curves. Consecutive treated cells showed slower decaying pair-correlation functions as compared to non-treated cells and cells that were pretreated with MβCD and LatB (Figure 4A). However, the difference between consecutive-treated cells and other treatments is less pronounced in the pair-correlation functions of CD20 (Figure 4B).

Unexpectedly, there was not a significant increase in CD20 cluster size or number of localizations per cluster in those cells treated with the nanoconjugates. The CD20 cluster size of the consecutive group is double the cluster size of the cells treated with Fab′-MORF1

Author Manuscript Author Manuscript Author Manuscript Author Manuscript

only. Previously, Chan et al., reported that CD20 migrates to lipid rafts after crosslinking.[17] We showed that using small molecules to prevent aggregation of lipid raft-associated molecules reduces apoptosis induction. Cholesterol serves as a spacer between sphingolipids and hydrocarbon chains, acting as glue for the lipid raft cluster. Without cholesterol, large lipid clusters did not form. Therefore, kinases associated with lipid rafts may be prevented from interaction with CD20 proteins. The use of MβCD and LatB decreased CD20 cluster size from a radius of 200 nm to 100 nm and 150 nm, respectively (Figure 4C).

Furthermore, we studied the 2-step in vivo targeting efficacy of the nanoconjugates in mice. Confocal microscopy was performed on excised portions of mouse tissues to investigate colocalization of Fab′-MORF1 with P-MORF2 on the B-cell surface. Raji cells (labeled with APC) were found in the lung, spleen, liver, and calvarium (Figure 5). Both Fab′-MORF1 and P-MORF2 co-localized with Raji cells in vivo (Figure 5). Higher magnification images showed that co-localization is indeed occurring on the surfaces of Raji cells.

We found that lipid raft cluster size correlated with apoptotic efficiency; however, CD20 cluster radii were not significantly greater than negative controls. Lipid raft clusters had radii ~200 nm in cells treated with the nanoconjugates, but when treated with lipid raft disrupting molecules the cluster size decreased to below 100 nm. We also found that even in the complex tissue environment in vivo, hybridization between the nanoconjugates occurred, and No non-specific co-localization of the conjugates was found in the imaged tissues, which supports the conclusion that this therapeutic system is highly specific.

Supplementary Material

Refer to Web version on PubMed Central for supplementary material.

Acknowledgments

Research reported in this publication was supported by the National Cancer Institute of the National Institutes of Health under Award Number F31CA186237 (to J.M.H.), NIH grant R01GM95606 (to J.K.) from the National Institute of General Medical Sciences and by NSF grant CHE-1306204 (to J.M.H.). The content is solely the responsibility of the authors and does not necessarily represent the official views of the National Institutes of Health and National Science Foundation. We would like to thank Eddie Hujber and Manasa Gudheti for guidance in dSTORM sample preparation and protocol optimization

References

1. Kopeček J. Mol Pharm. 2010; 7:922–925. [PubMed: 20672864]
2. Kopeček, J.; Kopečková, P. Drug Delivery in Oncology. Kratz, F.; Senter, PD.; Steinhagen, H., editors. Wiley-VCH Weinheim; Germany: 2011. p. 483-512.
3. a) Wu K, Liu JH, Johnson RN, Yang JY, Kopeček J. Angew Chem Int Ed. 2010; 49:1451–1455.b) Wu K, Yang J, Liu J, Kopeček J. J Control Release. 2012; 157:126–131. [PubMed: 21843563] c) Chu TW, Yang J, Zhang R, Sima M, Kopeček J. ACS Nano. 2013; 8:719–730. [PubMed: 24308267] d) Zhang R, Yang J, Chu TW, Hartley JM, Kopeček J. Adv Healthc Mater. 201510.1002/adhm.201400679e) Chu T-W, Kopecek J. Biomater Sci. 201510.1002/admh.201400679
4. Kiick KL. Science. 2007; 317:1182–1183. [PubMed: 17761873]
5. Huang B, Babcock H, Zhuang X. Cell. 2010; 143:1047–1058. [PubMed: 21168201]

Author Manuscript Author Manuscript Author Manuscript Author Manuscript

6. a) Sengupta P, van Engelenburg SB, Lippincott-Schwartz J. Chem Rev. 2014; 114:3189–3202. [PubMed: 24417572] b) Heilemann M, van de Linde S, Schüttpelz M, Kasper R, Seefeldt B, Mukherjee A, Tinnefeld P, Sauer M. Angew Chem Int Ed. 2008; 47:6172–6176.c) Linde S, Kasper R, Heilemann M, Sauer M. Appl Phys B. 2008; 93:725–731.
7. a) Honerkamp-Smith AR, Veatch SL, Keller SL. Biochimica et Biophysica Acta (BBA) - Biomembranes. 2009; 1788:53–63. [PubMed: 18930706] b) Sengupta P, Jovanovic-Talisman T, Skoko D, Renz M, Veatch SL, Lippincott-Schwartz J. Nat Methods. 2011; 8:969–975. [PubMed: 21926998] c) Veatch SL, Machta BB, Shelby SA, Chiang EN, Holowka DA, Baird BA. PLoS ONE. 2012; 7:e31457. [PubMed: 22384026]
8. Torre LA, Bray F, Siegel RL, Ferlay J, Lortet-Tieulent J, Jemal A. CA Cancer J Clin. 2015; 65(2): 87–108. [PubMed: 25651787]
9. Deans JP, Li HD, Polyak MJ. Immunology. 2002; 107:176–182. [PubMed: 12383196]
10. Shan DM, Ledbetter JA, Press OW. Cancer Immunol Immunother. 2000; 48:673–683. [PubMed: 10752475]
11. Janas E, Priest R, Wilde JI, White JH, Malhotra R. Clin Exp Immunol. 2005; 139:439–446. [PubMed: 15730389]
12. George KS, Wu S. Toxicol Appl Pharmacol. 2012; 259:311–319. [PubMed: 22289360]
13. Semac I, Palomba C, Kulangara K, Klages N, van Echten-Deckert G, Borisch B, Hoessli DC. Cancer Res. 2003; 63:534–540. [PubMed: 12543813]
14. Ivanov A, Beers SA, Walshe CA, Honeychurch J, Alduaij W, Cox KL, Potter KN, Murray S, Chan CHT, Klymenko T, Erenpreisa J, Glennie MJ, Illidge TM, Cragg MS. J Clin Invest. 2009; 119:2143–2159. [PubMed: 19620786]
15. Kraft ML. Mol Biol Cell. 2013; 24:2765–2768. [PubMed: 24030510]
16. Hammadi M, Pers JO, Berthou C, Youinou P, Bordron A. Onco Targets Ther. 2010; 3:99–109. [PubMed: 20616960]
17. Chan HTC, Hughes D, French RR, Tutt AL, Walshe CA, Teeling JL, Glennie MJ, Cragg MS. Cancer Res. 2003; 63:5480–5489. [PubMed: 14500384]

Author Manuscript Author Manuscript Author Manuscript Author Manuscript

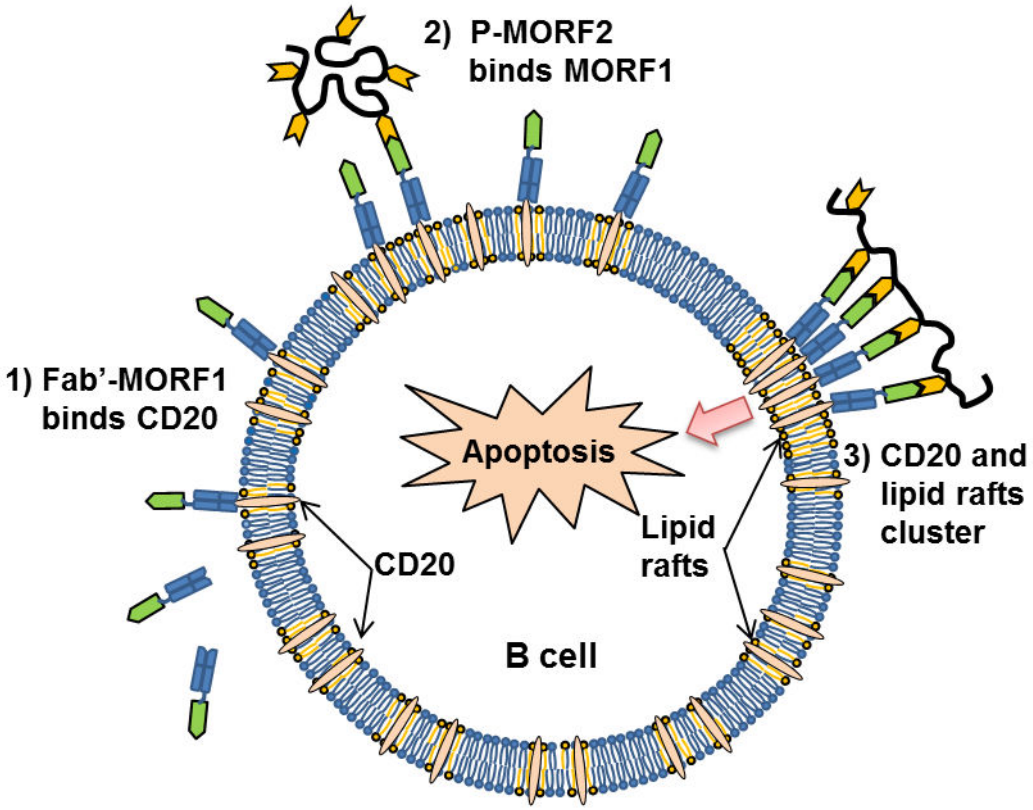

Figure 1.

Nanoconjugates hybridize on the cell surface stimulating lipid raft clustering thereby inducing apoptosis. 1) The anti-CD20 conjugate Fab′-MORF1 binds to CD20 and decorates the surface with MORF1 oligonucleotide; 2) The second nanoconjugate P-MORF2 hybridizes with MORF1; 3) Lipid rafts cluster in proximity to crosslinked CD20 proteins, thereby inducing apoptosis.

Author Manuscript Author Manuscript Author Manuscript Author Manuscript

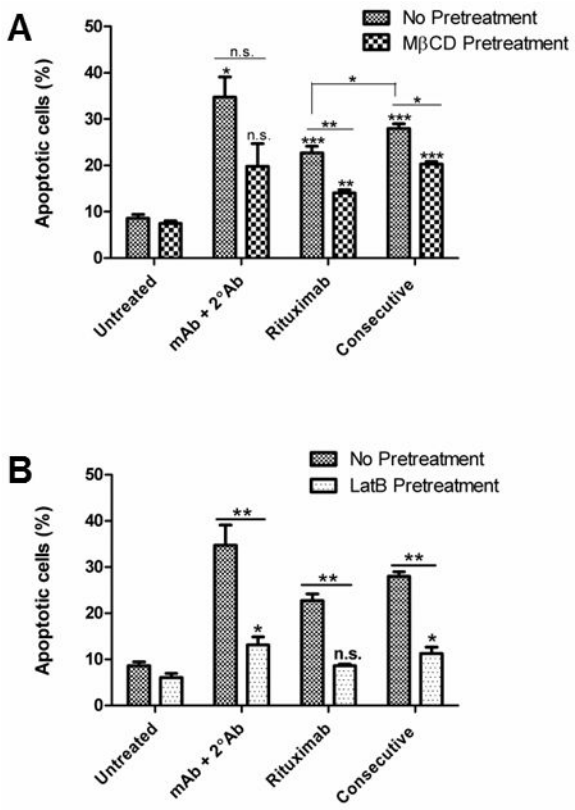

Figure 2.

Apoptosis induction and inhibition of Raji B-cells. The percentage of apoptotic cells was determined using an annexin V assay and quantified by flow cytometry. Cells were incubated for 6 h at 37 °C. Rituximab, mAb (1F5), and Fab′-MORF1 (consecutive) were administered at 1 μM concentrations based off molar concentration of Fab′. (A) Effects of pre-treatment with 10 mM MβCD for 15 min before incubation for 6 h. Untreated cells without therapeutic; mAb + 2°Ab, 1F5 mAb (1 μM) for 1 h followed by goat anti-mouse secondary Ab (0.5 μM); Rituximab (1 μM) for 1 h then washed; Consecutive, Fab′-MORF1 (1 μM) for 1 h followed by P-MORF2 (1 μM). The ratio of MORF1:MORF2 was 1:1. (B) Effect of pretreatment with 10 μM latrunculin B for 45 min on apoptosis. Significance was determined by comparing groups with untreated unless otherwise indicated (*$p < 0.05$, **$p < 0.005$, ***$p < 0.0001$, and n.s. indicates no significant difference).

Author Manuscript Author Manuscript Author Manuscript Author Manuscript

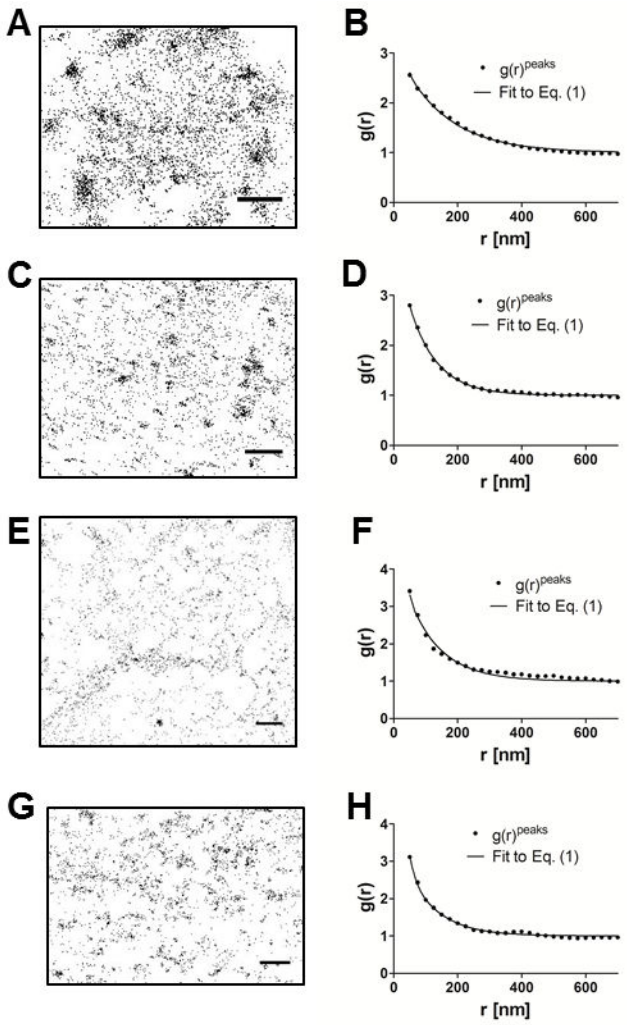

Figure 3.

dSTORM images and pair-correlation analysis. (A) CD20 distribution on the cell surface after 2 h consecutive treatment (Fab′-MORF1 and P-MORF2); (B, D, F, H) Pair-correlation function from images a, c, e, and g respectively fit to Equation 1; (D) Treatment with Fab′-MORF1; (E) LatB pretreatment then consecutive treatment; (G) MβCD pretreatment then consecutive treatment.

Author Manuscript Author Manuscript Author Manuscript Author Manuscript

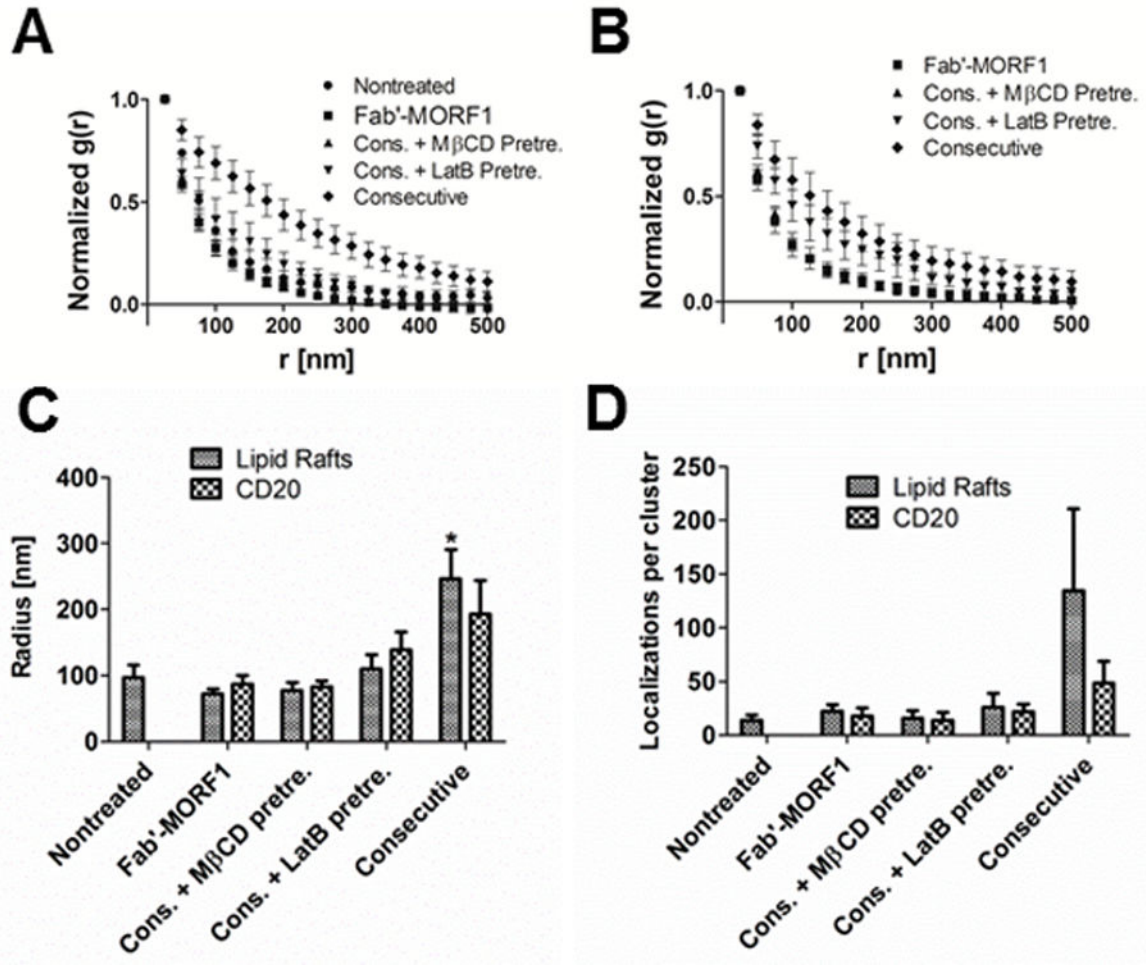

Figure 4.

Pair-correlation and cluster analysis. (A) Normalized pair-correlation functions of lipid raft distribution for different conditions, multiple images were acquired for each condition; (B) Normalized pair-correlation functions of CD20 distribution for different conditions; (C) Cluster radius values obtained from fitting data to equation 1; (D) Estimated number of localizations per cluster for the different conditions.

Author Manuscript Author Manuscript Author Manuscript Author Manuscript

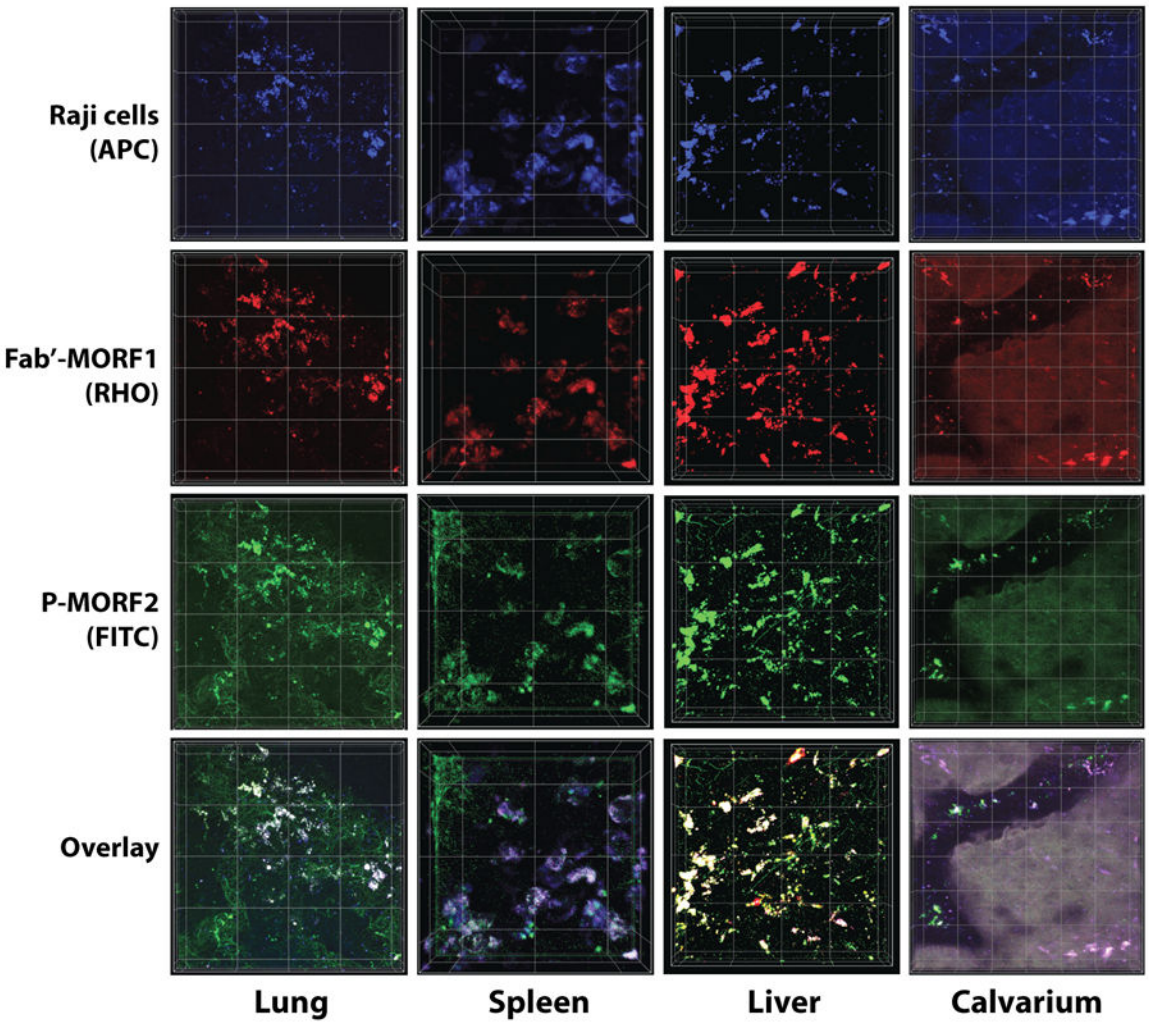

Figure 5.

In vivo tumor targeting in mice. 3D confocal microscopy analysis showed co-localization of three fluorescent signals indicating Raji cells (labeled with APC; blue), Fab′-MORF1 (labeled with rhodamine (RHO); red) and P-MORF2 (labeled with FITC; green). Raji cells were inoculated to SCID mice via the tail vein on day 1. On day 2, the mice were intravenously administered Fab′-MORF1, and, 5 h later, P-MORF2. Various tissues (as indicated) were harvested and imaged on day 5. Graticule size: 50 μm.

Author Manuscript Author Manuscript Author Manuscript Author Manuscript

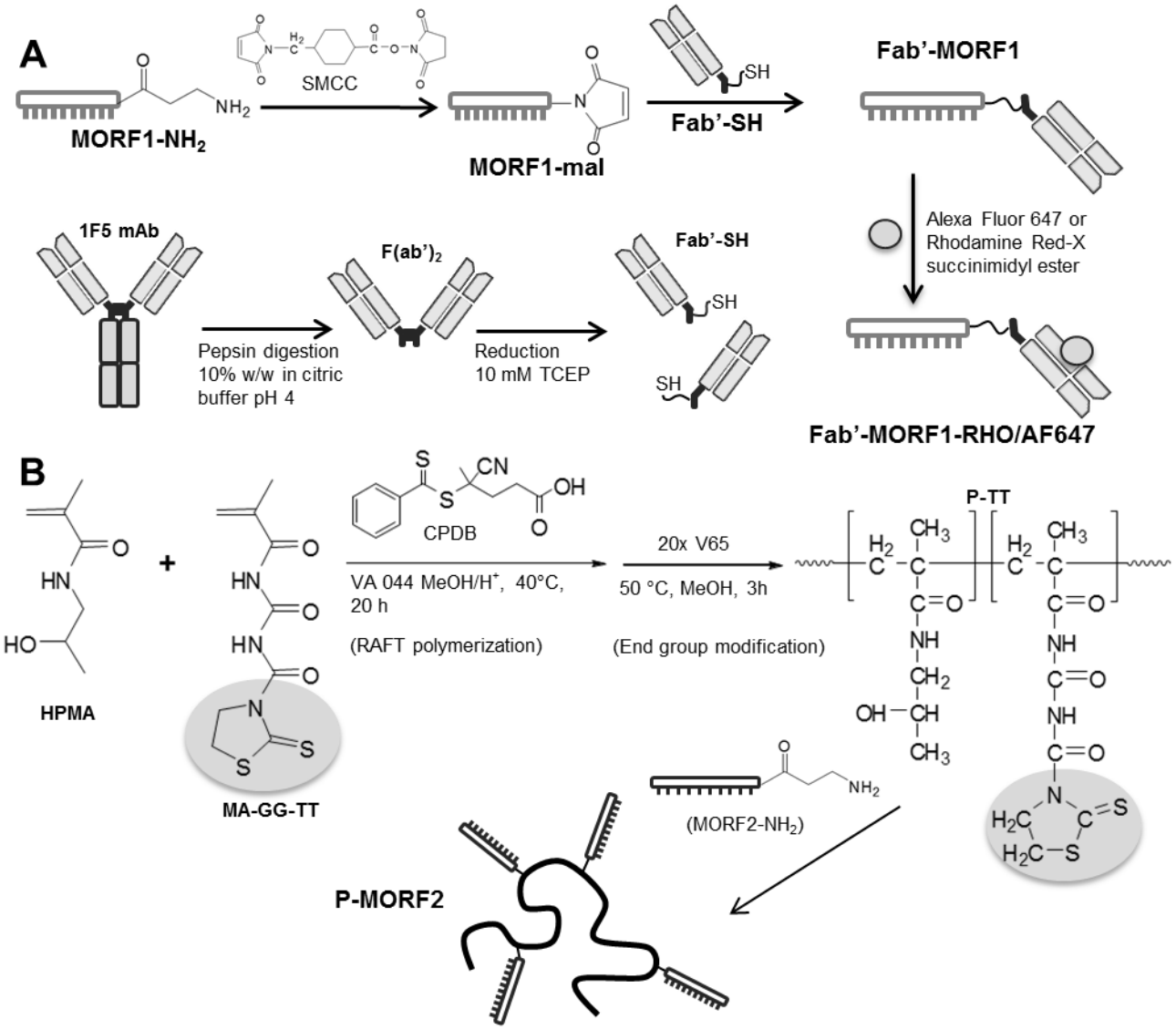

Scheme 1.

Synthesis of the nanoconjugates Fab′-MORF1, Fab′-MORF1-RHO/AF647, and P-MORF2. (A) Scheme of Fab′-MORF1 synthesis where MORF1-NH2 is reacted with succinimidyl-4-(N-maleimidomethyl)cyclohexane-1-carboxylate (SMCC) then reacted with Fab′-SH. (B) RAFT polymerization of the P-TT polymer and conjugation to MORF2-NH2.